1. Overview

Senior Personnel
Prof. C. Fred Driscoll, PI
Prof. Daniel H.E. Dubin, co-PI
Prof. Thomas O'Neil, collaborator

Project Scientists
Dr. Francois Anderegg
Dr. Andrey Kabantsev

1. Overview 1
2. a. IV: Laser-Diagnosed Mg+ 3
b. CamV: Camera-Diagnosed e^- and H^- 4
3. Magnetized Collisional Relaxation 6
a. Short- and Long-Range Collisions 6
b. Salpeter Correlation Enhancement 7
4. Transport Processes 9
a. Test Particle Diffusion 9
b. Velocity Slowing, "Noisy Caging" 10
c. Heat Conduction and Viscosity 11
5. Extrinsic Plasma Properties 14
a. Shear, Rotation, Boundaries 14
b. External Fields, Useful Work 15
c. Connecting with the Correlated Regime ... 16
6. Statement of Objectives 19
7. Current & Pending Support/Commitments .. 20

We propose experiments and theory characterizing the cross-magnetic field transport of particles and heat due to long-range collisions, extending from regimes of low-collisionality to regimes of moderate inter-particle correlation. The experiments will be performed on two existing, well-diagnosed research apparatuses. Theory characterizing the dynamics of collisional transport will be extended as appropriate, and quantitative comparison of theory and experiment will be obtained.

Experiments will be performed on two apparatuses: the "IV" apparatus contains Mg+ ion plasmas with sophisticated laser control and diagnostics, including "tagged" particle detection; and the "CamV" apparatus contains electron and H- plasmas, with accurate camera-based diagnostics. Most of the proposed funding is to support scientific staff and operational costs on these apparatuses.

The conceptual simplicity, long confinement times and excellent control of these cylindrical non-neutral plasmas has enabled incisive quantitative comparison of theory and experiment on many fundamental plasma processes. The long-term collaboration in theory and experiment between Driscoll, Dubin, and O'Neil has been recognized through many invited and plenary session lectures and through major APS awards. An important aspect of our experiments has always been the ability to vary plasma temperature over many decades, accessing different physical effects in different regimes.

Our prior research has made important advances in the theory and measurement of cross-field diffusion and heat transport in weakly-coupled plasmas. We have observed heat transport that is 2 orders of magnitude larger than predicted from classical (Braginskii) theory, but in agreement with new theory describing long-range collisions not included in the classical theory. These long-range collisions were also predicted to enhance cross-field diffusion, and these effects were measured in our experiments.

Here, we propose to extend our measurements of transport coefficients into regimes of moderate inter-particle correlation. On the IV machine, the strongly-coupled regime is readily accessed by laser-cooling; and recent laser upgrades now enable stable, quiescent plasmas with $T \sim 10^{-5}$ eV (0.1 Kelvin), giving correlation parameter $\Gamma \sim 10$. On the CamV machine, the research focus will be on wave/particle couplings, including the effects of disparate particle masses.

Also, we have broad experience in both the theory and investigation of strongly-coupled plasmas. Foundational work by group members described the thermal equilibrium states of trapped strongly-coupled non-neutral plasmas, including structural phase transitions and normal modes of plasma crystals [87], for which Dubin received the APS Excellence in Plasma Research Award.

In experiments, recent laser upgrades on IV enabled our measurements of the Salpeter enhancement of collisionality in plasmas with correlation parameter $0.1 \leq \Gamma \leq 20$. This represents the *only* experimental measurement of this effect, which is important in stellar fusion. The quantitative data fully supports "equilibrium shielding" theories, and contradicts recent "dynamical shielding" ideas.

In the strongly-correlated regime, and in the magnetized regime of $\Gamma_c > \Gamma_p$, the transport is primarily due to "long-range" collisions, extending over distances greater than a cyclotron radius; and this may include wave effects. Theory also distinguishes between the 3D regime where axial particle kinetics separates particles, and the 2D "bounce-averaged" regime where particles interact as charged "rods", until separated by ExB drifts across the magnetic field.

Our prior work characterized the dynamical effects of rotation, rotational shear, magnetic field strength, and plasma size on the transport, with different magnetic field scalings in the 2D and 3D regimes. We propose to extend these dynamical characterizations into the correlated regime, through analytic theory supported by small-scale simulations. The results will be connected with other groups' measurements of diffusion in un-magnetized, ultra-cold neutral plasmas; and with molecular-dynamics simulations of magnetized, strongly correlated plasmas.

Our prior theory and experiments identified the novel effects of "collisional caging", including enhanced particle slowing and enhanced cross-field diffusion. We propose to measure this enhanced velocity slowing in the weakly correlated regime of $T \sim 10^{-3}$ eV, of relevance to anti-matter trapping experiments.

Finally, we propose to extend our measurements of particle transport due to "external" couplings into lower temperature, correlated regimes, with theory interpretation where possible. External electric or magnetic couplings enable "useful work" to be transferred into or out of plasmas; and this is conceptually distinct from the "internal" collisional (i.e. dissipative) relaxation towards thermal equilibrium states. Our prior experiments show dramatic changes in external transport rates, depending on the "rigidity" ratio between axial particle bouncing rate and ExB drift-rotation rate. We will attempt to relate these results to magnetized plasma devices such as magnetrons and Hall thrusters, where transfer of useful work with minimal dissipative losses is desired.

2. Apparatuses

2a. IV: Laser-diagnosed Mg+ Plasmas

The IV apparatus (Fig. 1) contains unneutralized Mg^+ ions in rotating, near-thermal-equilibrium states, with sophisticated Laser-Induced Fluorescence (LIF) techniques providing diagnostics and control. The near-thermal-equilibrium Mg^+ ion plasmas have density $n = 10^6 - 10^8 \text{cm}^{-3}$, radii $R_p = 0.5 - 1.$ cm, and lengths $L_p = 1 - 30$ cm, with thermal energies ranging over $T = 10^{-5} - 10^0$ eV, in a magnetic field $B \le 3$ Tesla. Figure 2 shows typical steady-state equilibrium profiles of (a) density and temperature and (b) total drift velocity profile, with (calculated) diamagnetic contribution.

The ions are confined in steady-state for days or even weeks using the "rotating wall" technique [5-8], allowing transport measurements with unprecedented control and precision. This technique has now been adopted by (more than) 27 institutions world-wide [9-13], including the anti-matter recombination experiments at CERN. By varying temperature over 5 decades and density over 2 decades, the IV experiments provide strong tests of theory in many plasma regimes.

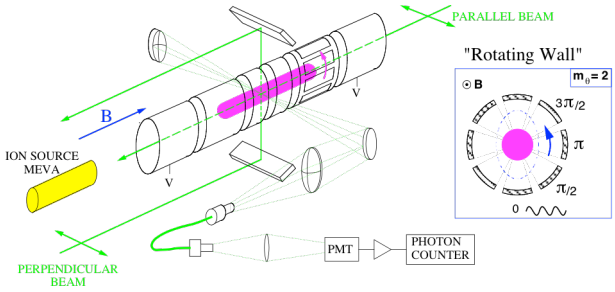

a)

Figure 1. IV Apparatus

b)

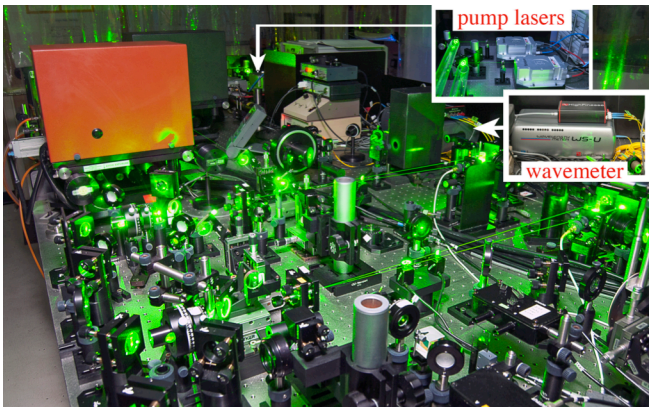

LIF diagnostic techniques allow time- and space-resolved measurement of density, temperature and rotation velocity; moreover, "test" particles can be "spin-tagged" and followed in time. A second beam is used to cool or heat the plasma or to manipulate the radial profile. Figure 1 shows the laser table: two tuneable CW dye lasers that are pumped by two solid state 10W 532 nm lasers. The dye lasers at 560 nm are frequency-doubled with two custom frequency-doubling cavities, producing two 10mW beams at ~280nm, which can be directed either along or across the plasma column. The control and diagnostics incorporates 9 racks of equipment and many special-purpose computer processes.

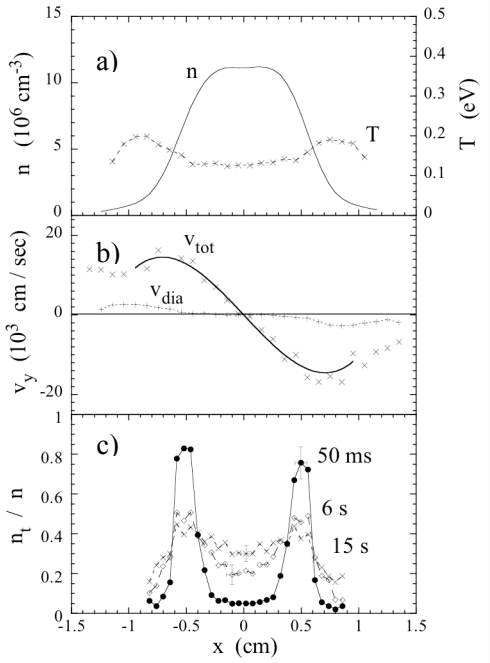

Figure 2. Example of Mg+ (a) density, temperature, (b) rotation velocity, and (c) tagged particle profiles

The frequency stability of the two lasers has recently been improved, to allow diagnostics and control to below 10^{-5} eV (~ 0.1 K). A sophisticated wavemeter (High Finesse WS-2) and feedback laser control reduces the laser frequency variability to $\Delta f / f \sim 4 \times 10^{-9}$, corresponding to Mg^+ thermal velocity at 4×10^{-7} eV (~ 4.mK). This extends our operating range from plasma ($\Gamma << 1$) to liquid ($\Gamma \approx 1$) to (at least) $\Gamma \gtrsim 20$, enabling transport measurements well into the correlated regime.

The IV apparatus was developed with ONR equipment funding of approximately $1.4M from 1990-1998. Continuing operation in our education-oriented program is

now partially funded by DOE Basic Plasma Science. The frequency stability upgrade was funded by the DOE High Energy Density Laboratory Plasma program.

Since inception, the IV apparatus has enabled quantitative comparison to theory on a broad range of basic plasma effects. The asterisks denote the first (or only) measurements of a specific effect.
* Salpeter enhancement of close collisions [42,43] (Sec 3b)
* Diffusion from long-range collisions [44] (Sec 4a)
* Heat transport from long range collisions [56] (Sec 4b)
* Shear reduction of collisional transport [3] (Sec 5a)
* Enhanced collisional drag from long-range collisions [52] (Sec 4b)
* Rotating Wall ∞-time confinement [5,6]
—Electron Acoustic Waves [14]
—Cyclotron modes in multi-species plasmas [15]
—Thermally-excited Langmuir modes [16]
—Linear Landau damping & trapping oscillations [17]
—Bounce-harmonic Landau damping of TG waves [18]

2b. CamV: Camera-diagnosed e- and H- Plasmas

The CamV apparatus utilizes a CCD camera to provide quantitative images of electron plasma density $n(r,\theta,t)$, and temperature $T(r,t)$, for both 2-dimensional (2D) $\mathbf{E}\times\mathbf{B}$ flow phenomena, and for 3D transport and damping effects associated with controlled magnetic and electrostatic separatrices.

The unneutralized electron plasma is trapped in a series of 15 cylindrical electrodes in an ultra-high vacuum environment. The electrons are contained axially by negative voltages on two end cylinders, and confined radially by a uniform axial magnetic field $B_z \le 2$ Tesla. The trapped electron column typically has density $n \sim 10^7$ cm^{-3}, radius $R_p \sim 1.5$ cm, and axial length $L_p \sim 50$ cm, with controlled temperatures in the range $0.03\text{eV} \lesssim T \lesssim 3\text{eV}$. Individual electrons bounce rapidly axially with low collisionality $\nu_{\perp\parallel} \approx 10-10^3$ sec^{-1}, and they $\mathbf{E}\times\mathbf{B}$ drift across the magnetic field. With large B, the electrons have an "inherent" confinement time of about 100.sec; and with the "rotating wall" technique, the confinement times can be extended to arbitrarily long times.

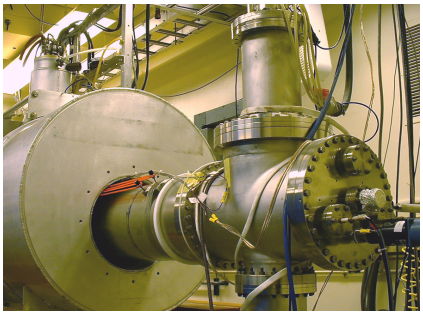

Figure 3. CamV Apparatus

At any desired time, the z-integrated electron density $n(r,\theta,t)$ is measured (destructively) by dumping the electrons axially onto a phosphor screen, which is imaged by a low-noise CCD camera. The 3D density $n(r,\theta,z,t)$ and self-consistent potential $\phi(r,\theta,z,t)$ can be constructed by assuming a Boltzmann equilibrium along each field line. The temperature $T(r,t)$ can be obtained from partial dumps over controlled electrostatic barriers. The shot-to-shot variations in the initial profiles are small, so the time evolution can be obtained from a sequence of shots with differing hold times. CamV incorporates about 7 racks of control and diagnostics electronics, as well as an extensive set of custom software programs, enabling fully quantitative measurements of subtle wave and transport effects.

2D Vortex Dynamics

The (r,θ) flow of "z-bounce-averaged" electrons is described by the 2D drift-Poisson equations, which are isomorphic to the Euler equations for an incompressible inviscid 2D fluid, with true free-slip radial and axial boundary conditions [19]. Only for fine spatial scales or long times (i.e. seconds), do collisional "viscous" or diffusive effects [23] become significant. Figure 4 shows an example of this *inviscid* self-organization of 2D vortices.

Major CamV results in this regime include :
* Formation of 2D turbulence to vortex crystals [26]
—vortex dynamics in background vorticity [30]
—inviscid symmetrization of vortices [30]
* fluid echoes from spatial Landau damping [31]

3D Kinetics

Contrasting with the inviscid fluid perspective is the axial kinetic regime, including subtle dissipative effects from separatricies induced by localized particle trapping. The resulting collisional and "chaotic" neoclassical transport (NCT) has recently been a primary research focus. Figure 5 is an example of the fully quantitative separatrix-induced transport rates ν observed from external perturbations ΔV_m versus controlled angle Θ_B [33].

Major results include:
* Chaotic NCT in parametric decay of drift waves [35]
* Separatrix-induced damping of diocotron waves [33]
* Separatrix-induced damping of θ-asymmetric BGK plasma waves [35]
—Superbanana particle transport in the low-collisionality regime [34]

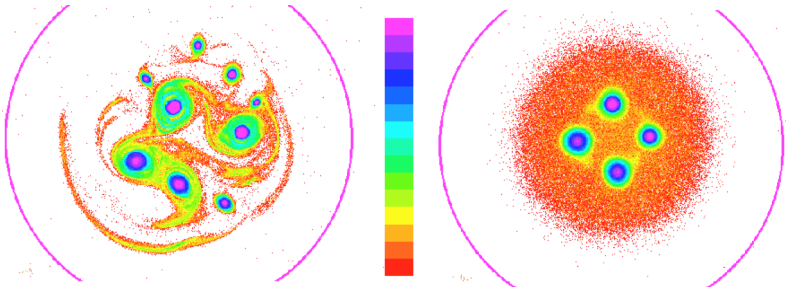

Figure 4. Example of 2D relaxation to vortex crystals

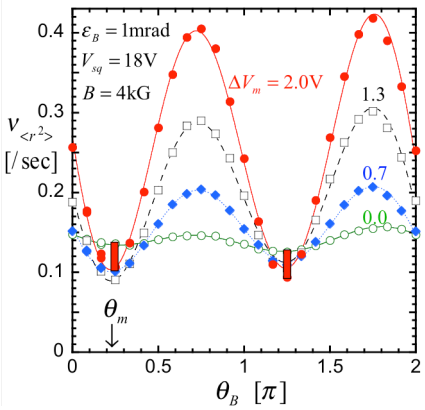

Figure 5. Example of separatrix-induced transport

3. Magnetized Collisional Relaxation

Here, we describe particle collisions in plasma which is at least moderately magnetized, i.e. with $\Omega_c > \omega_p$.

Parameters & notation (CGS)	
n [cm-3]	density
T [eV]	thermal energy
B [Gauss]	magnetic field
$a = (3/4\pi\, n)^{1/3}$	inter-particle spacing
$b = e^2 / T$	closest approach
$v_{th} = T / m$	thermal velocity
$\lambda_D = (T/4\pi ne^2)^{1/2}$	Debye length
$\Gamma = e^2 / a\, T$	correlation parameter
$\omega_p^2 = 4\pi ne^2/m$	plasma frequency
$\Omega_c = e\, B/mc$	cyclotron frequency
$r_c = v_{th} / \Omega_c$	cyclotron radius
$\kappa = \sqrt{2}\, b / r_c$	magnetization strength

3a. Short- and Long-Range Collisions

In weakly-correlated Maxwellian plasmas, the two-particle collision rate is given by $\nu_c = (8\sqrt{\pi}/15)\, n\, v_{th}\, b^2\, \ln\Lambda$, with Λ representing the ratio of the largest to smallest impact parameters ρ. Collisions divide into two impact-parameter ranges: "short-range" velocity-scattering collisions with impact parameters in the range $\rho < r_c$ as in Fig.6a; and "long-range" drift-kinetic collisions with $\rho > r_c$ as in Fig.6b. These two types of collisions have very different characteristics, and different scalings for transport coefficients.

For short-range collisions, the form of the Coulomb logarithm depends on the ratio r_c / b. When $r_c / b > 1$, then $\Lambda = r_c/b$. The velocity-scattering collisions in this regime (Fig. 6a) form the basis for "classical" transport theory developed for magnetic confinement fusion.

However, when $r_c / b < 1$ from strong magnetization, then the $\ln(r_c/b)$ approximation is inapplicable, and the perp-to-parallel scattering rate plummets, as shown in Fig. 7. Substantial theory work, and measurements on several apparatuses, has now characterized the *dynamical suppression* of perp-to-parallel equilibration due to a many-particle adiabatic invariant (the total cyclotron energy) [61]. This results in $\nu_{\perp//} \propto n\, v_{th}\, b^2 \exp\{ -\kappa^{2/5} \}$ for the strong magnetization regime of $r_c < b$. The exponential dependence on $\kappa \equiv \sqrt{2}\, b / r_c$ arises from an exponentially-small fraction of collisions that are sufficiently close, with $v_{//} / b \sim \Omega_c$, to break the adiabatic invariant. These rare super-thermal collisions dominate the equipartition rate.

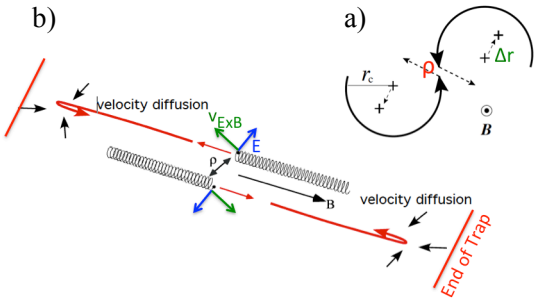

Figure 6. (a) Short-range velocity-scattering collision, and (b) long range drift-kinetic collision

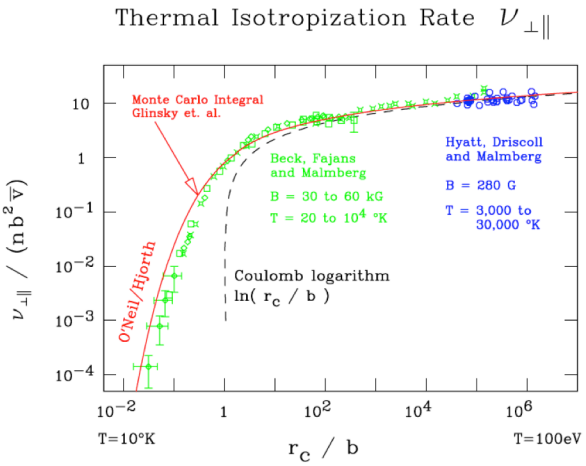

Figure 7. Dynamical suppression of perp-to-parallel collisions with strong magnetization.

On the other hand, long-range collisions with impact parameter ρ in the range $r_c < \rho < \lambda_D$ may also occur, in plasmas with $r_c < \lambda_D$. This regime is ignored in classical collision theory, but is common in low

density magnetized plasma and beam systems. These long-range collisions cause particle slowing and diffusion, heat transport, and viscosity, all without perp-to-parallel velocity scattering. In these collisions, there can be direct exchange of parallel energy, and small ExB drifts of the guiding centers as the particles stream past each other along B. Surprisingly, "collisional caging" effects substantially enhance the transport, even in the un-correlated ($\Gamma << 1$) regime, due to noise fluctuations and/or boundary effects. (sec 4a, 5a)

The transport resulting from these long-range collisions can be orders of magnitude larger than classical transport in weakly-correlated plasmas; for example, long-range cross-magnetic-field heat transport is *independent* of magnetic field. Note that this enhanced transport is due to collisions and thermal fluctuations, not to turbulence. Although the experiments described here are performed on non-neutral plasmas, the implications of the theory extend to plasmas in general.

3b. Correlation Enhancement of Energetic Collisions (Salpeter)

Our first experiments in the correlated regime characterized short-range collisions, specifically showing that inter-particle correlations *reduce the dynamical suppression* of perp-to-parallel equilibration shown in Fig.7; that is, correlations *enhance* $\nu_{\perp//}$. This turns out to be directly relevant to the substantially different parameters of stellar fusion.

In the 1950's, Salpeter predicted that fusion reaction rates in stars are enhanced by plasma screening [36]. The enhancement occurs because the plasma *screens* the Coulomb repulsion of the colliding ions, *enhancing* the probability of close collisions. Enhancement factors of roughly 4% - 5% are predicted for the parameters of the Sun; much larger enhancement factors are predicted for fusion in white dwarfs where the plasma is strongly correlated [37].

In the regime of $\Gamma << 1$, the Salpeter enhancement factor is $g(\Gamma) = \exp(\sqrt{3}\, \Gamma^{3/2})$ [43]. Recently there have been a number of papers [44-51] arguing that for $\Gamma << 1$ this standard Salpeter screening needs to be modified, or perhaps even neglected entirely, due to plasma effects associated with "dynamical screening." These theories try to account for the fact that the colliding ions are super-thermal, so their screening clouds are reduced and distorted by the high relative velocity of the colliding particles. However, others [37-41] argue that the Salpeter factor is an "equilibrium shielding" quantity determined by the static correlation function; and this implies that the enhancement is independent of the particles' relative velocity.

The rare energetic collisions causing stellar fusion are directly analogous to the rare energetic collisions causing perp-to-parallel scatterings in the strongly magnetized regime of Fig.7. Dubin formalized this isomorphism, showing that the same Gamov peak of collisionality occurs in both cases. This allowed us to make the *only* quantitative measurements of the Salpeter enhancement factor in a laboratory plasma [43], by measuring the perp-to-parallel collision rate $\nu_{\perp//}$ in the correlated regime of $\Gamma << 20$.

Figures 8a and 8b show the measured $\nu_{\perp//}$ versus temperature, with the lowest temperature measured ($T = 1\text{x}10^{-5}$ eV = 0.1 Kelvin) giving $\Gamma \sim 6$. The measured collisionality (red dots) is substantially enhanced over the "no correlation" curve, which is precisely the "κ-suppressed" curve of Fig. 7. This data set was taken to obtain high accuracy in the regime of $\Gamma \sim 1$, and it strongly contradicts the predictions of dynamical shielding.

In other data from IV, enhancement factors of up to 10^9 have been observed at $\Gamma \sim 20$, albeit with lower precision. Previously, similarly large $\nu_{\perp//}$ enhancements had been seen in crystalline ion clusters at NIST/Boulder, without a precise determination of T. For all measured Γ values, the data is fully

consistent with the "equilibrium shielding" predictions from several theory approaches. Moreover, the data is fully consistent with the theory result that the enhancement factor g(Γ) is *independent* of the magnetization parameter $\bar{\kappa} = \sqrt{2}\, b / r_c$, as it must be g(Γ) is truly an equilibrium property.

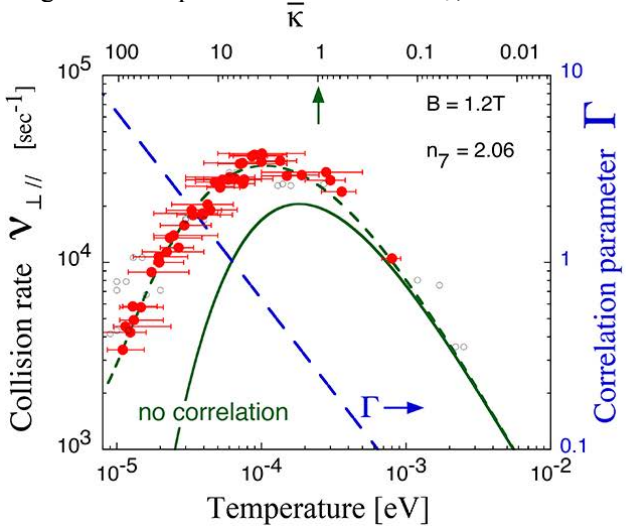

Figure 8a. Measured perp-to-parallel collisionality in the correlated regime.

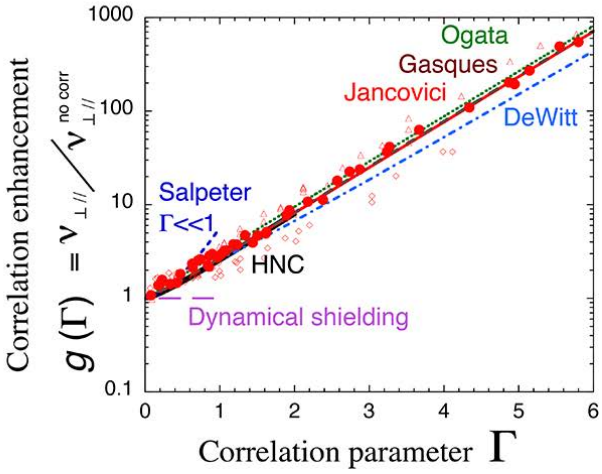

Figure 8b. Measured collisionality expressed as correlation enhancement.

4. Transport Processes

4a. Test Particle Diffusion, "Collisional Caging"

Our first measurements on the IV apparatus characterized test-particle diffusion at moderate temperatures, establishing the dominance of long-range collisions and "collisional caging". We propose to extend these measurements into the correlated regime. The experiments directly measure the cross-field diffusion of "tagged" particles versus time, to obtain the spatial diffusion coefficient $D_\perp$. The magnetic field makes the diffusion strongly an-isotropic, since collisions *reduce* $D_{//}$, but *enable* $D_\perp$

The data of Fig. 2c illustrates the technique. First, all ions are placed in the same spin state ("bleached"), using a cyclic transition. Then, at $t = 0$ almost all the ions at $r = 0.5$ are "tagged" into the opposite spin state. The cross-field density n_t of these tagged particles is then measured (non-destructively) versus time, with t = 50ms, 6sec, 15sec displayed here. As $t \rightarrow \infty$, $n_t(r)$ returns to (a fraction of) the steady-state profile shown in Fig. 2c. Detailed measurements and analysis establish that this is truly diffusive, rather than convective.

Figure 9 shows our initial $D_\perp$ measurements versus temperature T. The predicted and measured diffusion is proportional to density as n^1, and to magnetic field as B^{-2}, so these scalings are applied to the measurements before plotting, leaving only the dependence on (controlled) temperature T. The measured diffusion scales as $D_\perp \propto n^1 B^{-2} T^{-1/2}$, but is 10x larger than classical (short-range) collision predictions D_{class}, which is shown as a range depending on $\ln(\Lambda)$.

Surprisingly, the data was also 3x larger than the initial theory predictions for long-range collisions, labeled D_{3D}^{IUO}. This led (posthaste) to understanding the failure of the standard theory technique of "integration along unperturbed orbits" (IUO) for 1-dimensional collisions with noise, and to a 3x enhanced prediction D_{3D} [2]. Effectively, "collisional caging" causes each pair of particles to interact for 3x longer times than expected. This led recently to characterization of the fundamental length scale "d" separating binary "Boltzmann" collisions from noisy "Fokker-Planck" collisions, described in Sec(4b).

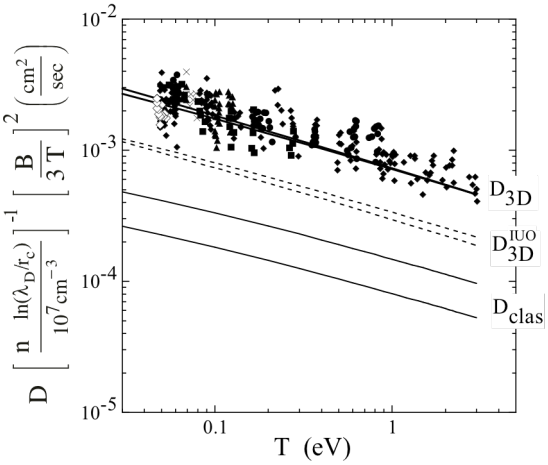

Figure 9. Measured test particle diffusion

=> We propose to extend these diffusion measurements to lower temperatures, where the ions become correlated. This requires simultaneously tagging and laser-cooling, which can be done with our existing two-laser system. Steady-state cooling to the desired plasma temperature will utilize the standard cyclic transition ($S_{1/2,mj=-1/2} \rightarrow P_{3/2,mj=-3/2}$) on the outer radial half of the plasma. The strong cooling also depopulates the ($S_{1/2,mj=+1/2}$) state, due to sideband pumping. The inner radial part of the plasma is then "tagged" into the ($S_{1/2,mj=+1/2}$) state. This tagged state is then non-destructively detected with a weak probe beam tuned to another cyclic transition ($S_{1/2,mj=-1/2} \rightarrow P_{3/2,mj=+3/2}$).

Recent simulations [82] have exhibited an interesting transition from the $D_\perp \propto B^{-2}$ to $D_\perp \propto B^{-1}$ as the plasma becomes strongly correlated. Our experiments will connect with this regime, as described in Sec.5c.

4b. Particle Velocity Slowing : "Collisional caging"

The parallel velocity slowing rate $\nu_{ss'}$ due to collisional drag is important to a number of processes, including the growth rate of non-ideal plasma instabilities, magnetic reconnection, runaway electrons, and anti-matter creation; however, a precise theory of the rate has only recently been formulated (and partially verified) for plasmas in the regime $r_c < \lambda_D$. Our new theory [52] and experiments [53] show that the collisional slowing rate $\nu_{ss'}$ can be considerably enhanced by long-range collisions.

Two classical theories of long-range collisions, Boltzmann and Fokker-Planck, give *different answers* for the slowing rate from long-range collisions between guiding centers moving in one dimension (1D), parallel to B [54]. In a Boltzmann collision, a colliding pair is assumed to be isolated; the total energy and parallel momentum are conserved. In a Fokker-Planck (FP) collision, many interactions are happening simultaneously, but each interaction is assumed to be weak.

Our new theory [52] shows that the discrepancy between the Boltzmann and Fokker Planck models is *resolved* by consideration of a novel but fundamental length scale

$$d \equiv ((e^2/\mu)^3 / D_{\|}^2)^{1/5}$$

Here $D_{\|}$ is the parallel velocity diffusion coefficient, related to $\nu_{ss'}$ by the Einstein relation $\nu_{ss'} = D_{\|}\, m / T$; and $\mu = m_s m_{s'} / (m_s + m_{s'})$. Collisions with impact parameter $\rho < d$ that result in reflections are sufficiently rapid to be treated as isolated Boltzmann collisions. But if $\rho > d$, reflections are slow enough so that velocity diffusion due to interactions with surrounding particles disrupts the reflection, requiring a FP theory analysis.

Thus, the theory predicts a slowing rate $\nu_{ss'} = \ln(\Lambda^*)$ with two additional Coulomb logarithms, as shown in Fig. 10a. The first logarithm arises from Boltzmann collisions with impact parameter ρ in the range $r_c < \rho < d$, and the second from FP collisions with impact parameters in the range $d < \rho < \lambda_D$. Interestingly, the coefficient of the Boltzmann term is zero for attractive interactions; but it equals 5.898 for repulsive interactions .

This computed coefficient is enhanced over naïve 1D Boltzmann theory (by a factor of 47%) by collisional caging: a repulsive Boltzmann collision between a particle pair does not occur only once; instead, it occurs as part of a *correlated sequence*. After one reflection, parallel velocity diffusion due to interactions with surrounding charges may cause the relative velocity of the pair to reverse, so that the pair collides again. The same velocity diffusion may also cause the particles to pass by rather than reflect, so their mutual correlation is lost. Figure 10b shows the predicted $\ln(\Lambda^*)$ for protons at $\{n=10^6, 10^7, 10^8\}$ compared to the classical (3D) Coulomb logarithm [54]. For $T \sim 10^{-3}$ to 10^{-1} the slowing is strong even though the classical rate goes to zero.

Our recent plasma wave damping experiments [53] on the IV apparatus have verified this enhanced drag due to long-range collisions. The experiments observe the damping rate of plasma waves in a multi-species ion plasma. Here, the species fractions are accurately measured by Thermal Cyclotron Spectroscopy, wherein small changes in the cooling laser fluorescence determine the resonant cyclotron frequency and density for each species.

At low temperatures, the wave damping is dominated by long-range collisional drag between the species: the heavy species react to the wave electric field less than the light species, and this difference in parallel velocities causes a frictional drag that damps the wave. Figure 10c shows that the measured damping is in (fair) quantitative agreement with the new theory (solid line), but up to 10x larger than classical theory (dashed line). These measurements span a range of 10^2 in temperature, down to $\Gamma \sim 1$ and $\kappa \sim 1$, where correlation effects are significant and the classical Coulomb logarithm is inapplicable.

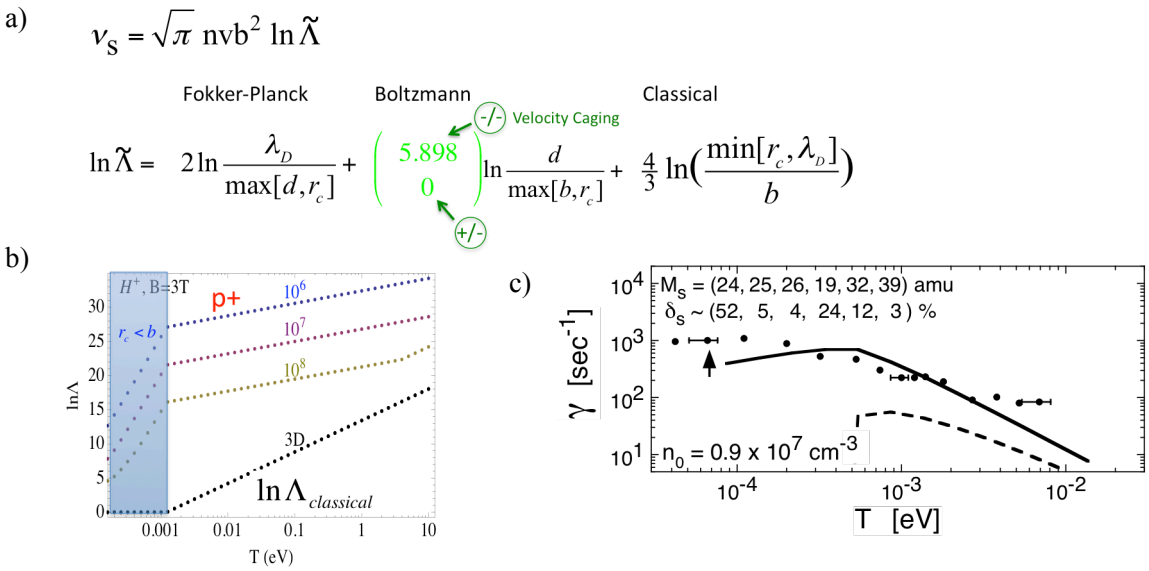

Figure 10. (a) Theoretical Coulomb logarithm terms; (b) Predicted enhancement for cryogenic proton plasmas; (c) Measured plasma wave damping

=> We propose to study the related process of parallel velocity diffusion of a particle distribution. An initially non-Maxwellian parallel velocity distribution will relax through collisional diffusion back to a Maxwellian at an enhanced rate due to long-range collisions. Such measurements have been made in neutral plasmas in the regime $r_c \gg \lambda_D$, [53] but when $r_c < \lambda_D$ new effects associated with long-range collisions occur. For example, for a single species plasma, long-range 2-body collisions do *not* affect the relaxation of the distribution (in theory) while 3D classical collisions do. This is because, for 1D collisions, two particles of the same species merely exchange parallel velocities, and this does not change the parallel distribution function for that species. In contrast, in a multiple species system, there *is* enhanced velocity diffusion from 1D long-range collisions, but only due to collisions between different species.

On the other hand, as the plasma becomes strongly correlated, same-species long-range collisions *do* cause parallel velocity diffusion, via 3-body collisions. We intend to search for signatures of this effect in our experiments, and to develop theory describing multi-body long-range collisions, for direct comparison to experimental velocity diffusion rates.

On IV, the collisional relaxation of the distribution functions of the three Mg^+ isotopes can be observed directly using our current laser diagnostic setup, and we propose to measure this relaxation to compare to theory that includes long-range collisions between species.

=> Velocity diffusion also plays a critical role in dissipative processes enabled by a velocity-space separatrix between locally-trapped populations of particles. Prior experiments and theory [32-35] have characterized the strong wave damping and particle transport effects from electric and/or magnetic barriers which trap even small populations of particles, as exemplified by Fig.5. On CamV, controlled separatrix experiments will be performed in the cold electron ($T \sim 0.025$ - 0.5 eV) regime where enhanced slowing is predicted.

4c. Heat Conduction and Viscosity

Transport processes for heat and momentum are subtle, in that they do not necessarily involve the transport of particles. We intend to extend experimental measurements into the regime of moderate correlation, with theory development as appropriate.

Measurements of cross-field collisional heat transport on IV show a strong enhancement (up to 300× classical) due to long-range collisions [56], and the heat transport is not reduced by strong magnetic fields. Here, a radial thermal gradient is created in the ion column by shining a laser along the magnetic field. After turning off the heating, the temperature gradient relaxation is measured using a low intensity probe beam.

For 3D long-range collisions in a weakly-correlated plasma, the predicted thermal diffusivity is $\chi \equiv 2\kappa / 3n = 0.48 v_0 \lambda_D^2$; and this agrees reasonably well with the measurements over a range of 3 decades in temperature, as shown in Fig. 11. The heat transport mechanism in the theory is the *exchange of parallel kinetic energy* by interacting particles that are on field lines separated by up to λ_D. Interestingly, the heat diffusivity from long-range interactions is *independent of density and magnetic field*, scaling only with temperature as $T^{-1/2}$. All three scalings (*n,B,T*) are quite different than the classical theory prediction [57], shown as dashed curves depending on density and magnetic field.

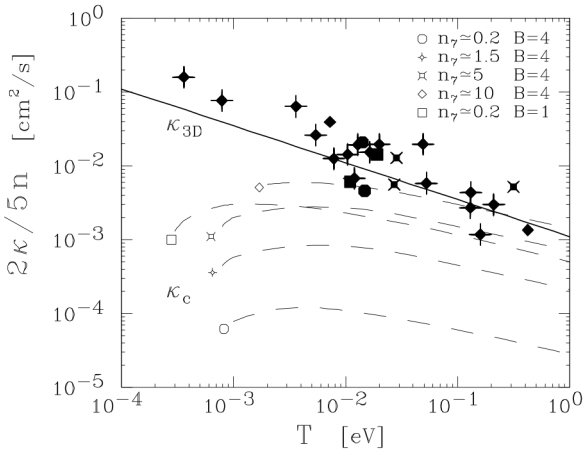

Figure 11. Measured heat conduction in un-correlated regime.

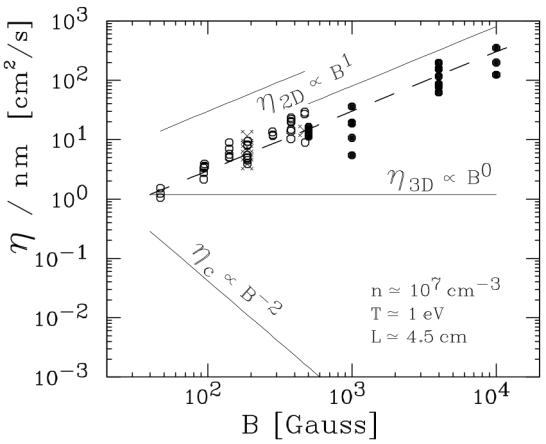

Figure 12. Measured viscosity compared to theoretical B-scalings

=> Our original measurements of $\chi(T)$ went down to T ~ 0.4meV, where $\Gamma \sim 1/6$. With improved laser stability, we intend to extend these measurements well into the correlated regime. In simulations of heat conduction in a weakly-magnetized, strongly-correlated plasma, there have been hints of a magnetic-field-independent region [84]. We intend to simulate heat conduction in larger magnetic fields, as appropriate to our experiments.

There can also be a contribution to χ from wave-mediated interactions between particles separated by very long distances ($\rho >> \lambda_D$), i.e. phonons in solids. In plasmas, this mechanism was originally considered by Rosenbluth and Liu [58] as a possible explanation of the anomalous heat loss through the electron channel in fusion plasmas. However, more theory work needs to be done in order to understand the effect of collisional damping of the plasma waves, which will become an important effect at low temperatures.

=> We intend to measure this wave-mediated heat transport on IV plasmas, where at sufficiently low temperature (i.e. when $R_p > 10^2 \lambda_D$) it is predicted to become the dominant heat transport process. For typical Mg^+ densities of $n \sim 2 \times 10^7$ cm^{-3}, this regime is readily accessed by T ≤ 1.meV (10.Kelvin).

Viscosity is the most dramatically non-classical of the transport coefficients, with measured enhancements up to 10^6 over classical theory [25]. As seen in Fig. 12, the classical coefficient scales as $\eta \propto B^{-2}$, whereas long-range theory gives $\eta \propto B^0$ in the 3D regime, and $\eta \propto B^1$ in the 2D bounce-averaged regime of low shear, as discussed below. These measurements are all from electrons in CamV, with T ~ 1.eV.

=> We intend to revisit these electron measurements with CamV room-temperature electrons ($\Gamma \sim 0.002$); and to compare to ion viscosity measurements on IV over the range $0.01 < \Gamma < 5$. We anticipate that data from the extended parameter ranges will provide substantial guidance to theory development.

5. Extrinsic Plasma Properties
5a. Dependence on Shear, Rotation, Boundaries

In magnetized, weakly-correlated laboratory plasmas, even near-thermal-equilibrium states exhibit transport coefficients depending on the rotation $\omega(r)$ or rotational shear $S \equiv r\,\partial\omega/\partial r$, and on external boundary conditions such as the plasma length L_p. The external boundaries are especially important when one considers useful work delivered to or from the plasma.

The surprising effects of rotational shear are clearly seen in our diffusion and viscosity measurements [3], and in the corresponding theory analyses [4]. For a confined plasma in a strong magnetic field, thermal particles bounce end-to-end at nearly-fixed {r,θ} position, with bounce frequency $f_{bou} \equiv v_{th} / 2L_p$. Two particles separated in radius by impact parameter ρ may then have $N_{bou} = f_{bou} / S$ correlated interactions before the shear separates them in θ by more than ρ.

For large f_{bou}, one may even envision a 2-particle collision as two "bounce-averaged" rods of charge taking {r,theta} steps away from their mean-field 2D flow. This is the 2D Taylor-McNamara limit, in which all evolution times necessarily scale as $\tau_{2D} \propto B^{-1}$.

In this regime, diffusion results from thermally-excited "eddies", which can be as large as the entire plasma R_p (Taylor-McNamara transport), unless limited by shear with smaller length scale L_ω. Thus, the diffusion coefficient itself may scale with system size or with external influences.

Figure 13 shows the measured cross-field particle *diffusion* D_{meas} (scaled to predicted D_{3D}) versus N_{bou}, obtained from IV plasmas with various temperatures and various shear profiles. As N_{bou} increases, the diffusion transitions from 3D to 2D magnitudes, and the magnetic scaling transitions from $D \propto B^{-2}$ to $D \propto B^{-1}$. In Fig. 14, the measured *viscosity* coefficient η shows the same dependence on N_{bou}, transitioning from the theoretically predicted η_{3D} to $(1+N_{bou})$ times as large, with B-scaling transitioning from $\eta \propto B^0$ to $\eta \propto B^1$.

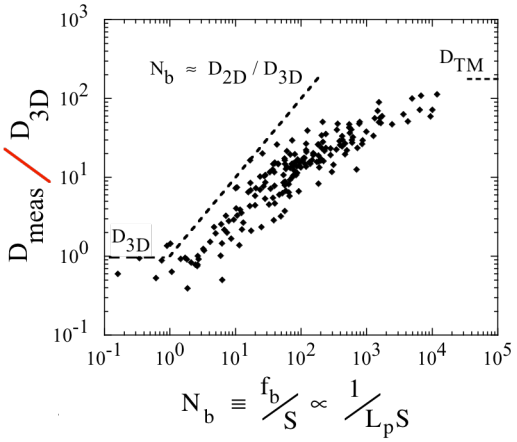

Figure 13. Bounce enhancement of diffusion

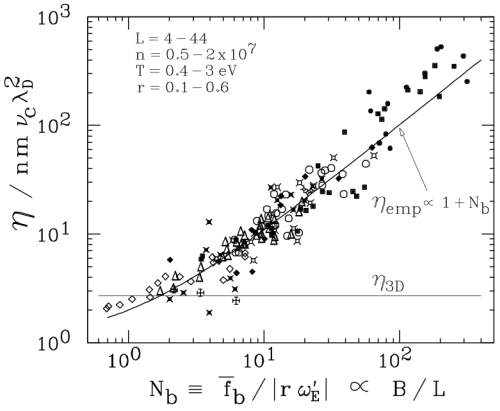

Figure 14. Bounce enhancement of viscosity.

This transition to $D_\perp \propto B^{-1}$ observed in our un-correlated plasmas may be connected to the transition to the B^{-1} scaling observed in simulations of strongly-correlated plasmas [82]. In both cases, the correlation time for collisional interactions is set by ExB drift dynamics, as charges drift across the magnetic field in

the electrostatic fluctuations produced by other particles. However, the simulations have no global shear flows (i.e. S=0). Realistic strongly-correlated plasmas might well have large-scale flows, and we intend to investigate shear effects in relation to realistic plasma systems.

5b. Interaction with External Fields, Useful Work

The prior section demonstrated that rotational shear, $S \equiv r\partial\omega/\partial r$, is a key parameter in determining the transport coefficients of diffusion and viscosity. Here, we demonstrate that absolute rotation $\omega(r)$ itself must be considered to understand dynamical couplings to the outside world. That is, delivering "useful work" into or out of a plasma invokes a substantially different perspective than does "relaxation to thermal equilibrium".

The transport processes described in previous sections arise from the plasma interacting with *itself*, often described as internal transport. The internal interactions conserve momentum, angular momentum, and even energy; but the entropy production (randomization) associated with the various types of collisions inevitably turns internal coherent energy into heat, with relaxation towards an isothermal, shear-free thermal equilibrium. For non-neutral plasmas and (idealized) One Component Plasmas, the well-understood thermal equilibrium states can be confined and provide a "reference model" linking the various dynamical processes.

Of equal importance in practical terms is how the plasma interacts with external structures and fields, i.e. "external transport". Non-neutral plasma thermal equilibria may approximate "the beam in the beam frame" in a free-electron laser; but the beam interaction with external structures (e.g. wigglers) invokes dynamics distinct from the thermal equilibrium perspective. Similarly, the electrostatic energy input to a magnetron generates ExB drift flow past RF cavities and flows out as EM waves; but the energy lost to vortex fluctuations and heat depends on flow dynamics and instabilities. Hall thrusters present even more challenging geometries, requiring controlled cross-field ExB drift flow of electron with simultaneous strong axial acceleration of ions. Thus, we intend to revisit various external transport processes from both the experimental and theoretical perspectives.

A prototypical external transport experiment is to determine the plasma expansion rate which is induced by a controlled θ-asymmetry in an external voltage (or magnetic field). This turns out to depend fundamentally on the plasma "rigidity", defined as the ratio of thermal particle bounce rate to ExB drift rotation rate, $R \equiv 2\pi\, f_{bou} / \omega_{ExB}$.

Indeed, Fig. 15 shows the measured expansion rate [91] scaling as R^{-2} in the low-rigidity regime, consistent across different apparatuses, magnetic fields, and densities. For R > 10, however, the expansion rate decreases abruptly by 2 decades, and becomes *independent of magnetic field*. At present, this abrupt suppression of the dominant transport process with strong magnetization at moderate temperature is not understood.

=> We intend to experimentally characterize the transport from various external perturbations, connecting the high temperature results with lower temperatures where stronger collisionality and inter-particle correlations become important.

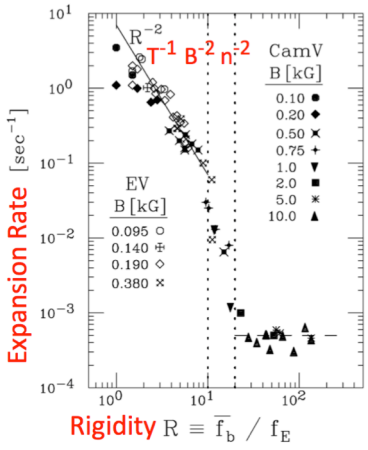

Figure 15. Electron plasma expansion from external couplings

5c. Connecting the Regimes

We propose to extend our magnetized plasma transport measurements into the correlated regime, making quantitative connection to experimental measurements and computer simulation results from other groups. We expect that this will develop new physics insights, and we will develop coherent theory perspectives where possible.

From the simplest theory perspective, the thermal equilibrium plasma properties depend only on density, temperature and applied magnetic field { n, T, B }, which determine many one component plasma (OCP) characteristics such as collisionality, correlations, and waves. Adding Yukawa shielding from a second (highly mobile) species makes the YOCP somewhat more tractable, while still relevant to many forms of esoteric matter.

As shown above, the description of practical magnetized plasmas must also include "dynamic" parameters such as rotation and shear, axial bounce frequencies, fraction non-neutrality, and overall plasma radius and length, i.e. { ω, $r\partial\omega/\partial r$, f_{bou}, δ_q, R_p, L_p }. Moreover, many of these parameters significantly affect the magnetic field scaling $\{B^0, B^{-1}, B^{-2}\}$, even relatively near to thermal equilibrium. In this section we highlight some of the similarities and disparities between regimes, where we hope to contribute further connections.

Crystal Stasis

Pure ion crystals can now be routinely contained, imaged, and manipulated, primarily due to developments by the time-standards and quantum-computing groups of John Bollinger and Dave Wineland at NIST/Boulder. In this program, UCSD "post-doc exports" enabled stroboscopic single-ion imaging using the rotating wall technique [7]; imaging of the spheroidal plasma modes [88] which had been analytically characterized by Dubin [87]; and this included identification of the "external drags" arising from plasma modes which are zero-frequency in the lab frame. Recently, Dubin [59] has contributed an analysis of the "triangular pancake" crystal equilibria in rotating wall stasis, which may be useful for creating controllable "engineered spins" as quantum Qbits.

The external drags on these strongly-correlated rotating equilibria are counter-balanced by the rotating wall fields. This has a cost of some added entropy, so understanding and minimizing the external transport processes would be useful.

=> We plan to extend the expansion rate measurements of Fig. 15 into the cryogenic regime with ($0.001 \leq \Gamma \leq 2$). There, the stronger collisionality presumably kills the "rigidity dynamics" of Fig. 15, and causes the expansion rate to *decrease* with further decreasing temperature. Here, experimental data will be useful in developing a much-needed theoretical overview reaching into the correlated regime.

Anti-matter, Multiple species

Accumulation and storage of positrons and anti-protons has become a mature technology, culminating in the recent creation and trapping of low-energy anti-hydrogen by the ALPHA [12] and ATRAP [13] groups. The Surko positron trap has become a standard worldwide, through extension of the rotating wall strategy into the high-density, low-slip "strong drive" regime [8], aided in theory by O'Neil. Anti-hydrogen formation in strong magnetic fields includes a stage of "guiding center atoms" [60-64], wherein cyclotron dynamics strongly constrains the collisional energy equipartition (as in Fig. 7). Substantial theory and simulation work on the development of two-body correlations (i.e. re-combination) contributed to today's highly optimized techniques for anti-hydrogen production.

Centrifugal separation of heavy and light species (both of the same charge sign) is becoming important in many traps; e.g. electron cooling of anti-protons [69,70]. The radial separation develops when the centrifugal energy difference between species is comparable to thermal energy T, i.e. $\Delta m\, \omega_r^2\, R_p^2 / T \geq 1$. This is directly analogous to liquid/crystal correlations developing when the inter-particle electrostatic energy is comparable to T , i.e. $\Gamma = (e^2/a) / T \geq 1$. The equilibrium theory of centrifugal separation is well-understood [65], and the standard collisional transport rate has been calculated [67]. However, experiments typically observe separation in substantially shorter times than predicted from collisions, albeit not yet quantitatively measured.

Recent experiments with e^- / H^- plasmas on CamV [66] have observed strongly enhanced centrifugal separation when the fundamental $k_z=0$, $m_\theta=1$ diocotron mode is present, at even small amplitues. The outward H^- transport rate is proportional to the diocotron mode amplitude, and there is concurrent diocotron mode damping. At present, there is no theoretical understanding of this dynamical process, but it is apparently another example of wave or instability dynamics causing transport and rapid relaxation to a lower energy state.

=> Given the ubiquity of diocotron modes in nonneutral traps, this wave-induced centrifugal transport process is probably quite common. We intend to extend these experiments on CamV, and ideally to develop a quantitative theory perspective connecting the collisional and wave-induced regimes.

Ultra-Cold Neutral Plasmas

The ultra-cold neutral plasma community has had considerable success in creating, diagnosing, and simulating the correlated plasma states which develop concurrent with plasma expansion. In UCNPs, experimental control of the overall charge non-neutrality δ_q (through the electron temperature T_e) determines the expansion and recombination rates [76,77]; and the adiabatic expansion has been well characterized experimentally and theoretically [71,73,74] Importantly, the fast electrons determine the Debye shielding for the system. The minimal ion temperature is determined by de-correlation heating [72,73], although continued laser cooling has been proposed.

In UCNPs, both ion acoustic waves (IAW) and electron plasma waves have been measured. For IAW experiments [75], plasma expansion caused the dominant wave damping; whereas for electron plasma waves, kinetic (Landau) damping dominated [89].

=> We will measure damping rates for Mg+ plasma waves and for diocotron modes at low temperatures, extending into the correlated regime. This will be in conjunction with particle diffusion measurements, discussed next.

Transport Coefficients in Correlated Regimes

Transport coefficients in correlated regimes have been primarily studied via One Component Plasma (OCP) simulations [79,80], and by effective potential theory [81], with UCNP experiments now also providing quantitative data for $D_{//}$ [78]. We believe that non-neutral plasma experiments will provide a strong "reality anchor" to simulations, especially in identifying the various dynamical processes which converge into the strongly collisional regime of $\Gamma = 1$, where the collisionality is maximal, at $\nu_c \sim \omega_p$.

=> Cross-field particle diffusion $D_\perp$ is a basic spatial transport coefficient, which we propose to measure between the low-collisionality and correlated regimes. Figure 16 gives a "correlation-oriented" overview of $D_\perp$ experiments and simulations to date. Here, our prior measurements (from Figs. 9 and 13 re-scaled) in the strong shear regime of $N_{bou}\sim 1$ are shown as solid circles; our measurements with reduced rotational shear (N_{bou} = 2 to 2000) are shown as color-coded X's; and some simulation results of Ott and Bonitz

(scaled for density and magnetic field) are shown as open circles [82]. The strong-shear NNP results scale as $D_\perp \propto B^{-2} T^{-1/2}$, and a $T^{-1/2}$ extrapolation plausibly "connects" with simulation results for the correlated regime.

In contrast, no theory perspective exists for extrapolating the low-shear $D_\perp$ measurements into the correlated regime. There are, however, encouraging similarities: the simulations [82] show a scaling transition from $D_\perp \propto B^{-2}$ to $D_\perp \propto B^{-1}$ with increasing magnetization; and other simulations have analyzed "particle caging" [83], which may be the high-collisionality limit of the "collisional caging" observed in NNPs (Sec.4a,4b). Here, our proposed experiments will be compared directly to supported theory and targeted (small-scale) simulations, and to results of other groups.

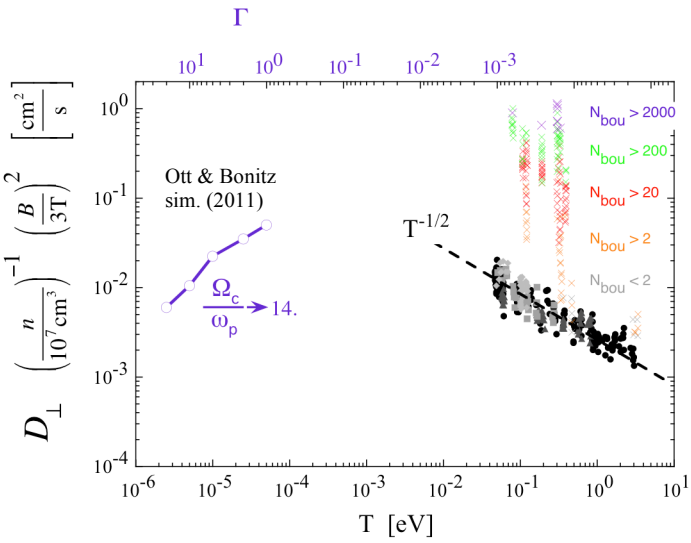

Figure 16. Dynamical effects in diffusion at high T will be connected to simulation results at low T.

=> The proposed cross-field heat transport measurements will extend into the $\Gamma \sim 1$ regime, and extrapolation of the $\chi \propto T^{-1/2}$ scaling of Fig. 11 gives $\chi \sim \omega_p a_{ws}^2$, as expected for collisionality $\nu_c \sim \omega_p$ and shielding $\lambda_D \sim a$, corresponding to recent YOCP simulations [90]. Yet to be understood is the heat transport effect of plasma waves, predicted to be dominant when $R_p \geq 100\lambda_D$ for weak correlation (Sec4c). The proposed experiments will explore this wave-transport regime, if high densities from the rotating wall can be combined with 10^{-5} eV temperatures obtained from our improved laser stability.

6. Statement of Objectives

Experiments will be performed on two existing, well-diagnosed magnetized plasma devices. On the IV apparatus, Mg+ ions will be laser-cooled over the range $10^{-5} < T < 1.$ eV , allowing fundamental plasma transport processes to be quantitatively characterized into the correlated regime. On the CamV apparatus, pure electron plasmas and e^-/H^- plasmas will be studied over the range $.025 < T < 1.$eV, characterizing ExB drift particle dynamics, and drift-wave/particle-transport interactions. Where possible, further theory perspectives will be developed and quantitatively tested with the experimental data.

Specifically:

1) Experiments will extend measurements of cross-field particle diffusion, $D_\perp$, from the low-collision regime into the correlated regime of $\Gamma \geq 1$, characterizing the dynamical effects of rotational shear and finite-size/boundary effects. Results will be compared to MD simulations and to UCNP experiments in the correlated regime.

2) Experiments will test Dubin's recent theory predicting enhanced collisional slowing of particles due to noise-induced "collisional caging" in long-range collisions. Experiments will focus on the weakly correlated T~1.meV energy range.

3) Experiments will extend measurements of cross-field heat conductivity, κ , from the low-collisional regime into the correlated regime. Where significant conductivity from waves is predicted, experimental data will be compared quantitatively to theory.

4) Experiments will measure the enhanced centrifugal transport of H^- in electron plasmas, due to coupling between particle transport and the fundamental center-of-mass diocotron mode. Explanatory theory will be developed and tested.

5) As they develop, new theory perspectives on collisional transport in the 2D and 3D regimes will be related to other fields of physics, from fluid dynamics to space plasmas; and to practical devices, from cryogenic anti-matter containment to energetic Hall thrusters.

- **It is understood that any developmental items and specially designed parts, components, accessories and attachments fabricated under any Department of Defense award resulting from this proposal are being developed for both civil and military applications.**

Current and Pending: Time Support / Time Commitment

Current

DOE DE-SC0018236 Fundamental Processes in Plasmas					
$400,000 / yr 15-Aug-2017 → 14-Aug-2020	Driscoll	Dubin	O'Neil	Anderegg	Kabantsev
	0. / 2. PI	0.5 / 2. co-PI	0. / 1	5.2 / 5.2	5.2 / 5.2
DOE DE-SC0008693 Experiments and Theory on KEEN Waves and the Salpeter Screening Enhancement					
$220,000 / yr 1-Jul-2017 → 1-Jul-2018	Driscoll	Dubin	O'Neil	Anderegg	Kabantsev
	0.3 / 1. PI	0.3 / 1. co-PI	0.3 / 1	2.8 / 2.8	---

Bibliograhy & References

Test Particle Diffusion

1. F. Anderegg, X.-P. Huang, C.F. Driscoll, E.M. Hollmann, T.M. O'Neil, and D.H.E. Dubin, "Test Particle Transport due to Long-Range Interactions," Phys. Rev. Lett. **78**, 2128 (1997).

2. D.H.E. Dubin, "Test Particle Diffusion and the Failure of Integration Along Unperturbed Orbits," Phys. Rev. Lett. **79**, 2678 (1997).

3. C.F. Driscoll, F. Anderegg, D.H.E. Dubin, D.-Z. Jin, J.M. Kriesel, E.M. Hollmann, and T.M. O'Neil, "Shear Reduction of Collisional Transport: Experiments and Theory," Phys. Plasmas **9**, 1905 (2002).

4. D.H.E. Dubin, "Collisional Diffusion in a 2-Dimensional Point Vortex Gas or a 2-Dimensional Plasma," Phys. Plasmas **10**, 1338 (2003).

IV Apparatus, "Rotating Wall"

5. X.-P. Huang, F. Anderegg, E.M. Hollmann, C.F. Driscoll and T.M. O'Neil, "Steady-State Confinement of Non-neutral Plasmas by Rotating Electric Fields," Phys. Rev. Lett. **78**, 875 (1997).

6. F. Anderegg, E.M. Hollmann, and C.F. Driscoll, "Rotating Field Confinement of Pure Electron Plasmas Using Trivelpiece-Gould Modes," Phys. Rev. Lett. **78**, 4875 (1998).

7. X.-P. Huang, J.J.Bollinger, T.B. Mitchell, W.M. Itano, and D.H.E. Dubin, "Precise control of the global rotation of strongly coupled ion plasmas in a Penning trap," Phys. Plas. **5**, 1656 (1998)

8. J.R. Danielson, C.M. Surko, and T.M. O'Neil, "High-Density Fixed Point for Radially Compressed Single-Component Plasmas," Phys. Rev. Lett. **99**, 135005 (2007)

9. D. B. Cassidy, V. E. Meligne, and A. P. Mills, Jr., "Production of a Fully Spin-Polarized Ensemble of Positronium Atom", Phys. Rev. Lett. **104**, 173401 (2010)

10. V. Nosenko, A. V. Ivlev, S. K. Zhdanov, M. Fink and G. E. Morfill, " Rotating electric fields in complex (dusty) plasmas", Phys Plasmas **16**, 083708 (2009)

11. N.Kuroda & ASACUSA collaboration, "Radial Compression of an Antiproton Cloud for Production of Intense Antiproton Beams", Phys Rev Lett **100**, 203402 (2008)

12. G. B. Andresen and the ALPHA Collaboration, "Compression of Antiproton Clouds for Antihydrogen Trapping", Phys. Rev. Lett. **100**, 203401 (2008)

13. G. Gabrielse and the ATRAP Collaboration, "Adiabatic Cooling of Antiprotons", Phys. Rev. Lett. **106**, 073002 (2011)

14. F. Anderegg, C.F. Driscoll, D.H.E. Dubin, and T.M. O'Neil, "Wave-Particle Interactions in Electron Acoustic Waves in Pure Ion Plasmas", Phys. Rev. Lett. **102**, 095001 (2009).

15. M. Affolter, F. Anderegg, D.H.E. Dubin and C.F. Driscoll, "Cyclotron Mode Frequency Shifts in Multi-species Ion Plasmas" Physics Letters A **378**, 2406 (2014)

16. F. Anderegg, N. Shiga, J.R. Danielson, D.H.E. Dubin, and C.F. Driscoll, "Thermally Excited Modes in a Pure Electron Plasma," Phys. Rev. Lett. **90**, 115001 (2003).

17. J.R. Danielson, F. Anderegg and C.F. Driscoll, “Measurement of Landau Damping and the Evolution to a BGK Equilibrium,” Phys. Rev. Lett. **92**, 245003 (2004).

18. F. Anderegg, M. Affolter, A.A.Kabantsev, D.H.E.Dubin, A.Ashourvan, C.F.Driscoll, "Bounce Harmonic Landau Damping of Plasma Waves," Physics of Plasmas **23**, 055706, (2016).

CamV Apparatus

19. C.F. Driscoll and K.S. Fine, “Experiments on Vortex Dynamics in Pure Electron Plasmas,” Phys. Fluids B **2**, 1359 (1990).

20. A.J. Peurrung and J. Fajans, “A Limitation to the Analogy between Pure Electron Plasmas and 2-D Inviscid Fluids,” Phys. Fluids B **5**, 4295 (1993).

21. N.S. Pillai and R.W. Gould, “Damping and Trapping in 2D Inviscid Fluids,” Phys. Rev. Lett. **73**, 2849 (1994).

22. T.M. O'Neil, “A New Theory of Transport due to Like Particle Collisions,” Phys. Rev. Lett. **55**, 943 (1985).

23. C.F. Driscoll, J.H. Malmberg and K.S. Fine, “Observation of Transport to Thermal Equilibrium in Pure Electron Plasmas,” Phys. Rev. Lett. **60**, 1290 (1988).

24. D.H.E. Dubin, “Collisional Transport in Nonneutral Plasmas,” Phys. Plasmas **5**, 1688 (1998).

25. J. M. Kriesel and C. F. Driscoll, “Measurements of Viscosity in Pure-Electron Plasmas”, Phys. Rev. Lett. **87**, 135003 (2001).

26. K.S. Fine, A.C. Cass, W.G. Flynn, and C.F. Driscoll, “Relaxation of 2D Turbulence to Vortex Crystals,” Phys. Rev. Lett. **75**, 3277 (1995).

27. D.Z. Jin and D.H.E. Dubin, “Regional Maximum Entropy Theory of Vortex Crystal Formation,” Phys. Rev. Lett **80**, 4434 (1998).

28. D.Z. Jin and D.H.E. Dubin, “Characteristics of Two-Dimensional Turbulence that Self-Organizes into Vortex Crystals,” Phys. Rev. Lett. **84**, 1443 (2000).

29. D.A. Schecter and D.H.E. Dubin, “Vortex motion driven by a background vorticity gradient,” Phys. Rev. Lett. **83**, 2191 (1999).

30. 174.D.A. Schecter, D.H.E. Dubin, A.C. Cass, C.F. Driscoll, I.M. Lansky, and T.M. O'Neil, “Inviscid Damping of Asymmetries on a Two-Dimensional Vortex,” Phys. Fluids **12**, 2397 (2000).

31. J.H. Yu, T.M. O'Neil, and C.F. Driscoll “Fluid Echoes in a Pure Electron Plasma”, Phys. Rev. Lett. **94**, 025005 (2005).

32. D.H.E. Dubin and Yu.A. Tsidulko "Neoclassical transport and plasma mode damping caused by collisionless scattering across an asymmetric separatrix," Phys. Plasmas **18**, 062114 (2011).

33. C.F. Driscoll, A. A. Kabantsev, D.H.E. Dubin and Yu.A. Tsidulko "Overview of Transport, Damping, and Wave Couplings from Separatrix Dissipation in an Axisymmetric Plasma," Trans. of Fusion Sci. and Tech. **59**, 170 (2011); Open Systems 2010 Conference, Novosibirsk.

34. D.H.E. Dubin, A.A. Kabantsev and C.F. Driscoll "Enhanced superbanana transport caused by chaotic scattering across an asymmetric separatrix," Phys. Plasmas **19**, 056102 (2012).

35. A.A. Kabantsev and C.F. Driscoll "Trapped-Particle-Mediated Collisional Damping of Non-Axisymmetric Plasma Waves," Phys. Rev. Lett. **97**, 095001 (2006); "Chaotic Neoclassical Separatrix Dissipation in Parametric Drift-Wave Decay," Phys. Rev. Lett. 112, 055003, 2014.

Salpeter Correlation Enhancement

36. E.E. Salpeter, "Electron screening and thermonuclear reactions," Australian J. Phys. **7**, 373 (1954).

37. J.N. Bachcall, L. S.Brown, A. Gruzinov, and R. F. Sawyer, "The Salpeter plasma correction for solar fusion reactions," Astronomy and Astrophysics **383**, 291 (2002)

38. S. Ichimaru, "Nuclear Fusion in Dense Plasmas," Rev. Mod. Phys. **65**, 255 (1993).

39. S. Ichimaru and H. Kitamura, "Pycnonuclear Reactions in Dense Astrophysics and Fusion Plasmas," Phys. Plas. **6**, 2649 (1999).

40. H. Dewitt and W. Slattery, Contrib. Plas. Phys. 39, 97 (1999) ; A. Chugunov, H. E. DeWitt, and D. G. Yakovlev, Phys. Rev. D **76**, 025028 (2007)

41. S. Ogata, "Enhancement of Nuclear Reaction Rates in Dense Stellar Matter: A Path-Integral Monte Carlo Simulation Study," Astrophys. J. 481, 883 (1997); S. Ogata, H. Iyetomi, and S. Ichimaru, "Nuclear Reaction Rates in Dense Carbon-Oxygen Mixtures," Astrophys. J. **372**, 259 (1991)

42. D.H.E. Dubin "Measurement of Screening Enhancement to Nuclear Reaction Rates Using a Strongly-Magnetized and Strongly-Correlated Non-neutral Plasma," Phys. Rev. Lett. **94**, 025002 (2005)

43. F. Anderegg, D.H.E. Dubin, M. Affolter, C.F. Driscoll "Measurements of Correlations-Enhanced Collision Rates in the Mildly Correlated Regime", Physics of Plasmas, **24**, 092118 (2017); SciLight **2017**, 140007 (2017)

44. C. Carraro, A. Schafer, and S. E. Koonin, "Dynamic screening of thermonuclear reactions," Astrophys. J. **331**, 565 (1988).

45. G. Shaviv and N. J. Shaviv, "Is there a dynamic effect in the screening of nuclear reactions in stellar plasmas?" Astrophys. J. **529**, 1054 (2000); J. Shaviv and G. Shaviv, "The electrostatic screening of thermonuclear reactions in astrophysical plasmas," Astrophys. and Space Sci. Lib. **214**, 43 (1997); N. J. Shaviv and G. Shaviv, "The electrostatic screening of thermonuclear reactions in astrophysical plasmas. I.," Astrophys. J. **468**, 433 (1996).

46. V. I. Savchenko, "Quantum, multibody effects and nuclear reaction rates in plasmas," Phys. Plasmas **8**, 82 (2001).

47. N. Tsytovich, "Suppression of thermonuclear reactions in dense plasmas instead of Salpeter's enhancement," Astron. and Astrophys. **356**, L57 (2000).

48. M. Opher and R. Opher, "Dynamic screening in thermonuclear reactions," Astrophys. J. **535**, 473 (2000).

49. A. Lavagno and P. Quarati, “Nonextensive statistics in stellar plasma and solar neutrinos,” Nucl. Phys. B (Proc. Suppl.) **87**, 209 (2000).

50. A. Weiss, M. Flaskamp, and V. N. Tsytovich, “Solar models and electron screening,” Astron. and Astrophys. **371**, 1123 (2001).

51. D. Mao, K. Mussack and W. Dappen, “Dynamic Screening in Solar Plasma”, Ap. J. **701**, 1204 (2009); D. Mussack and W. Dappen, “Dynamic Screening Correction for Solar p-p Reaction Rates,” Ap. J. **729**, 96 (2011).

Transport and Velocity Slowing

52. D.H.E. Dubin, “Parallel Velocity Diffusion and Slowing Down Rate from Long Range Collisions in a Magnetized Plasma”, Phys. Plasmas **21**, 052108, (2014)

53. M. Affolter, F. Anderegg, D.H.E. Dubin and C.F. Driscoll, “First Test of Long-Range Collisional Drag Via Plasma Wave Damping”, Phys. Rev. Lett. **117**, 155001 (2016)

54. T. M. O’Neil, “Collision Operator for a Strongly Magnetized Pure Electron Plasma”, Phys. Fluids **26**, 2128 (1983)

55. J. Bowles, R. McWilliams and N. Rynn, “Direct Measurement of Velocity-Space Transport in a Fully ionized Plasma”, Phys. Rev. Lett. **68**, 1144 (1992)

56. E.M. Hollmann, F. Anderegg, and C.F. Driscoll, “Measurement of Cross-Magnetic-Field Heat Transport in a Pure Ion Plasma,” Phys. Rev. Lett. **82**, 4839 (1999)

57. M.N. Rosenbluth and A.N. Kaufman, Phys. Rev. **109**, 1 (1958)

58. M.N. Rosenbluth and C.S. Liu, Phys. Fluids **19**, 815 (1976)

Devices and Technologies

59. D.H.E. Dubin, "Structure of two-dimensional plasma crystals in anharmonic Penning traps", Phys. Rev. A **88**, 013403 (2013).

60. M.E. Glinsky and Thomas M. O'Neil, "Guiding Center Atoms: Three-body Recombination in a Strongly Magnetized Plasma," Phys. Fluids B **3**, 1279 (1991)

61. M.E. Glinsky, T.M. O'Neil, M.N. Rosenbluth, K. Tsuruta and S. Ichimaru "Collisional Equipartition Rate for a Magnetized Pure Electron Plasma," Phys. Fluids B **4**, 1156 (1992)

62. C.F. Driscoll, "Comment on Driven Production of Cold Antihydrogen and the First Measured Distribution of Antihydrogen States," Phys. Rev. Lett. **92**, 149303 (2004)

63. D.H.E. Dubin, "Electronic and Positronic Guiding Center Ions," Phys. Rev. Lett. **92**, 195002 (2004)

64. E.M. Bass and D.H.E. Dubin, "Relaxation of Antihydrogen from Rydberg to Ground State," AIP Conf. Proc. **862**, 147 (2006)

65. T.M. O'Neil "Centrifugal Separation of a Multispecies Pure Ion Plasma," Phys. Fluids **24**, 1477 (1981)

66. A.A. Kabantsev and C.F. Driscoll "First Experiments with e-/H- Plasmas: Enhanced Centrifugal Separation from Diocotron Mode Damping," submitted, NNP-2017 Proceedings .

67. D.H.E. Dubin "Equilibrium and Dynamics of Multispecies Nonneutral Plasmas with a Single Sign of Charge," Non-Neutral Plasma Physics VIII, AIP Conf. Proc. **1521**, 26-34 (2013).

68. D.H.E. Dubin "Electrostatic waves and instabilities in multispecies nonneutral plasmas," Phys. Plasmas **17**, 112115 (2010).

69. G.B. Andresen, ALPHA Collaboration, " Centrifugal Separation and Equilibration Dynamics in an Electron-Antiproton Plasma", PRL **106**, 145001 (2011).

70. G. Gabrielse, ATRAP Collaboration, "Centrifugal Separation of Antiprotons and Electrons", PRL **105**, 213002 (2010).

UNCP and Simulations

71. A.V. Baitin and K.M Kuzanyan "A self-similar solution for expansion into a vacuum of a collisionless plasma bunch," J. Plasma Physics, **59**, 83 (1998)

72. S.G. Kuzmin and T.M. O'Neil "Numerical Simulation of Ultracold Plasmas: How Rapid Intrinsic Heating Limits the Development of Correlation," Phys. Rev. Lett. **88**, 065003 (2002).

73. F. Robicheaux and J.D. Hanson, "Simulated expansion of an ultra-cold, neutral plasma", Phys. Plasmas **10**, 2217 (2003).

74. D. Vrinceanu, G.S. Balaraman and L.A. Collins, "The King model for electrons in a finite-size ultracold plasma," J. Phys. A: Math. Theor. **41**, 425501 (2008)

75. T.C. Killian, P. McQuillen, T.M. O'Neil and J. Castro, "Creating and studying ion acoustic waves in ultracold neutral plasmas," Phys. Plasmas **19** 055701 (2012).

76. Craig Witte and J.L. Roberts, "Ultracold plasma expansion as a function of charge neutrality", Phys. Plasmas **21**, 103513 (2014); "Evaluation of charged particle evaporation expressions in ultracold plasmas," Phys. Plasmas 24, 052122 (2017).

77. Tianxing Chen, R. Lu, Li Guo, and S. Han, "The charge imbalance in ultracold plasmas", Phys. Plasmas **23**, 092102 (2016).

78. T.S. Strickler, T.K. Langin, P. McQuilen, J. Daligault, and T.C. Killian, "Experimental Measurement of Self-Diffusion in a Strongly Coupled Plasma", Phys. Rev. X **6**, 021021 (2016).

79. J. Daligault, K. Rasmussen and S.D. Baalrud, "Determination of the shear viscosity of the one-component plasma", Phys. Rev. E **90**, 033105 (2014).

80. S.D. Baalrud and J. Daligault, "Transport Regimes Spanning Magtnetization-Coupling Phase Space", Phys. Rev. E **96**, 043202 (2017).

81. S.D. Baalrud and J. Daligault, "Effective Potential Theory for Treansport Coefficients across Coupling Regimes", Phys. Rev. Lett **110**, 235001 (2013).

82. T. Ott and M. Bonitz, "Diffusion in a Strongly Coupled Magnetized Plasma", Phys. Rev. Lett **107**, 135003 (2011).

83. K.N. Dzhumagulova, R.U. Masheyeva, T. Ott, P. Hartmann, T.S. Ramazanov, M. Bonitz, and Z.Donko, "Cage correlation and diffusion in strongly coupled three-dimensional Yukawa systems in magnetic fields", Phys. Rev. E **93**, 063209 (2016).

84. T. Ott, M.Bonitz, and Z. Donko, "Effect of correlations on heat transport in a magnetized strongly coupled plasma", Phys. Rev E **92**, 063105 (2015); T. Ott *et al*, "Recent Progress in the theory and simulation of strongly correlated plasmas," Eur. Phys. J. D. 72:84 (2018)

85. C.L. Ellison, Y. Raitses, and N.J. Fisch, "Cross-field electron transport induced by a rotating spoke in a cylindrical Hall thruster", Phys. Plasmas **19**, 013503 (2012).

86. T. Lafleur, S.D. Baalrud, and P.Chabert, "Theory for the anomalous electron transport in Hall effect thrusters: I. Insights from particle-in-cell simulations", Phys Plasmas **23**, 053502 (2016); "II. Kinetic model", Phys. Plasmas **23**, 053503 (2016)

Additional

87. D.H.E. Dubin "Theory of Electrostatic Fluid Modes in a Cold Spheroidal Nonneutral Plasma," Phys. Rev. Lett. **66**, 2076 (1991)

88. T.B. Mitchell, John J. Bollinger, W.M. Itano, J.M. Kriesel, and D.H.E. Dubin "Doppler Velocimetry of Cryogenic Ion Plasmas," IEEE Trans. on Plasma Science **30**, 16 (2002).

89. Wei-Ting Chen, Craig Witte, and Jacob L. Robert "Damping of electron center-of-mass oscillations in ultracold plasmas," Phys. Plasmas **23**, 052101 (2016)

90. S.D. Baalrud and J. Daligault "Transport Regimes Spanning Mangetization-Coupling Phase Space," Phys. Rev E **96**, 043202 (2017)

91. J.M. Kriesel and C.F. Driscoll, "Two Regimes of Asymmetry-Induced Transport in Non-neutral Plasmas", Phy. Rev. Lett **85**, 2510 (2000).